IVYSPRING INTERNATIONAL PUBLISHER

Theranostics

2017; 7(19): 4689-4698. doi: 10.7150/thno.21672

Research Paper

CO_2-based amphiphilic polycarbonate micelles enable a reliable and efficient platform for tumor imaging

Yuanyuan Li[1, 2], Shunjie Liu[2, 3], Xun Zhao[3], Ying Wang[1, 2], Jianhua Liu[4]✉, Xianhong Wang[2, 3]✉ and Lehui Lu[1, 2]✉

1. State Key Laboratory of Electroanalytical Chemistry, Changchun Institute of Applied Chemistry, Chinese Academy of Sciences, Changchun 130022, China
2. University of Chinese Academy of Sciences, Beijing 100049, China
3. Department Key Laboratory of Polymer Ecomaterials, Changchun Institute of Applied Chemistry, Chinese Academy of Sciences, Changchun 130022, China
4. Department of Radiology, Second Hospital of Jilin University, Changchun, 130041, China

✉ Corresponding authors: Prof. L. H. Lu E-mail: lehuilu@ciac.ac.cn; Prof. X. H. Wang E-mail: xhwang@ciac.ac.cn; Dr. J. Liu E-mail: drliujh@yahoo.com

Received: 2017.06.28; Accepted: 2017.09.01; Published: 2017.10.17

Abstract

Biodegradable polymeric nanomaterials can be directly broken down by intracellular processes, offering a desirable way to solve toxicity issues for cancer diagnosis and treatment. Among them, aliphatic polycarbonates are approved for application in biological fields by the United States Food and Drug Administration (FDA), however, high hydrophobicity, deficient functionality and improper degradation offer significant room for improvement in these materials. Methods: To achieve progress in this direction, herein, we demonstrate that CO_2-based amphiphilic polycarbonates (APC) with improved hydrophilicity and processability can be used as a reliable and efficient platform for tumor imaging. To better investigate their potential, we devised a convenient strategy through conjugation of APC with gadolinium (Gd). Results: The resulting polymeric micelles (APC-DTPA/Gd) exhibit excellent magnetic resonance imaging performance, simultaneously enabling real-time visualization of bioaccumulation and decomposition of polymeric micelles *in vivo*. Importantly, these micelles can be degraded to renally cleared products within a reasonable timescale without evidence of toxicity. Conclusion: Our findings may help the development of CO_2-based amphiphilic polycarbonate for cancer diagnosis and treatment, accompanied by their low-toxicity degradation pathway.

Key words: carbon dioxide, polycarbonate, biodegradable, renal clearance, imaging agents

Introduction

Nanomaterials circulating in the body have great promise for cancer diagnosis and treatment [1, 2]. However, to realize clinical translation, the fullest consideration must be given to their long-term toxicity [3-5]. An important strategy to minimize toxicity is to construct nanomaterials with harmless clearance characteristics within a reasonable amount of time [6-8]. For example, small-sized nanodots (hydrodynamic size <5.5 nm) that show efficient renal clearance could mitigate their toxic effect [9-11]. Unfortunately, rapid renal clearance decreases the time available to the nanomaterials to perform their diagnostic and/or therapeutic function. Moreover, optimized formulations can also leave residual by-products in mononuclear phagocytic system (MPS), especially heavy metals and toxic constituents [12]. To address these issues, efforts have been made to develop biodegradable polymer nanomaterials, which can be broken down by intracellular processes and rapidly eliminated from the body [13-17]. Based on the source, biodegradable polymers can be classified as biological or synthetic polymers. Although biologically derived biodegradable polymers such as polysaccharides and proteins have good bioactivity and accessibility to cell-triggered proteolytic degradation, most of these polymers face

practical limitions including a robust immunogenic response and the complexities related to their chemical modifications [18]. Thus, synthetic biodegradable polymers have become magnetic alternatives for bioapplications. Among them, aliphatic polycarbonates have received much attention due to their excellent biocompatibility, biodegradability, and approval for biomedicine use by the FDA [19-22]. Notably, polycarbonates suffer from surface erosion degradation *in vivo* rather than bulk degradation in the hydrolysis of aliphatic polyesters [23]. Importantly, polycarbonate degradation does not result in the formation of acids, which may be observed during polyester degradation, hence reducing the hazard of adverse reactions in bioapplications [24].

However, the commonly used aliphatic polycarbonates are formed according to the ring opening polymerisation of six-membered cyclic monomers, which suffer from high hydrophobicity, deficient functionality and improper degradation profile [25, 26]. Such an "inert" nature has largely hampered their design as imaging platforms. To overcome these limitations, we set out to employ the CO_2-based amphiphilic block polycarbonate (APC) as a platform for tumor imaging. The premise for our design is that APC can provide diverse and reactive groups, offering great opportunities for further modifications by conjugates with other interesting biofunctionalities. More importantly, facilely functionalized APC improves hydrophilicity and biodegradability, which assures clearance from the body in a reasonable timescale [27-29]. In addition, this alternative route from directive copolymerization of epoxides with CO_2, an abundant, nontoxic and noninflammatory C1 feedstock, eliminates the need of preparing toxic phosgene-derived monomers [30]. Taken together, CO_2-based polycarbonate is biologically and environmentally a more benign choice as a reliable platform for *in vivo* disease diagnosis. To better understand its potential, we explored the capacity of this platform for tumor imaging. A strategy was devised through conjugation of APC with gadolinium (Gd^{3+}). The resulting polymeric micelles (APC-DTPA/Gd) exhibited excellent magnetic resonance imaging performance, simultaneously enabling real-time visualization of bioaccumulation and decomposition of polymeric micelles *in vivo*. Importantly, these micelles can be degraded into renally cleared products within a reasonable timescale without evidence of toxicity. These results highlight a direction in the design of CO_2-based amphiphilic block polycarbonate with a low-toxicity degradation pathway for cancer diagnosis and treatment.

Materials and Methods

Materials

Reactions sensitive to oxygen or moisture were performed in a glovebox under Ar. Propylene oxide (99%, J&K) and 4-vinyl-cyclohexene-1, 2-epoxide (98%, TCI) were distilled over CaH_2 prior to use. Dimethoxy-2-phenylacetophenone (DMPA), L-cysteine, ditert-butyl dicarbonate, diethylenetriaminepentaacetic dianhydride (DTPA-BA) and $GdCl_3$ were purchased from TCI. Dichloromethane and toluene were distilled using CaH_2 and Na, respectively. Carbon dioxide (>99.9%) was used as received. Thiazolyl tetrazolium and sodium citrate tribasic dehydrate were purchased from Sigma-Aldrich. High-glucose DMEM medium and RPMI 1640 medium were purchased from Thermo Fisher Scientific. Fetal bovine serum was obtained from Gibco. Other reagents were used as received without any treatment. Ultrapure water (18.2 MU) used throughout this work was prepared by Milli-Q Academic (Millipore).

Synthesis of DTPA-labeled APC (APC-DTPA)

6 mmol of DTPA-BA in 30 mL of DMSO was added to an equimolar amount of APC (cysteine amount; the synthesis of APC is described in the supplementary experimental section), and the mixture was regulated to pH 7 by adding TEA. The temperature was increased to 70 °C and maintained for 3 h under N_2 protection. Then the product was precipitated in acetone, and the precipitate was dissolved in 20 mL of deionized water. After dialysis for 3 days, the APC-DTPA was lyophilized for further use.

Synthesis of APC-DTPA/Gd

To the APC-DTPA aqueous solution was added an equimolar amount of an aqueous solution of $GdCl_3$ dropwise under stirring for 1 h. The pH value of the reaction system was controlled to ~6.5 by adding NaOH. The solution was then subjected to dialysis until no free Gd^{3+} was detected. The samples were then lyophilized and dispersed in deionized water for 10 min to get assembled micelles.

Measurement of the critical micelle concentration (CMC) of APC and APC-DTPA/Gd

The CMC value of APC and APC-DTPA/Gd was measured using the hydrophobic probe pyrene by fluorescence spectroscopy with some modification [31]. 100 μL of pyrene solution at a concentration of 6 μM in acetone was added to the centrifugal tubes, and evaporated to dryness. Then 1.0 mL aqueous solution

of APC or APC-DTPA/Gd of different concentrations was added with vigorous shaking and kept overnight. Fluorescence emission from 360 nm to 400 nm was measured with an excitation of 334 nm. Finally, the intensities of the 373 nm and 392 nm peaks were calculated and fitted via Boltzamann analytical method.

In vitro degradation of APC and APC-DTPA/Gd

The size change of the micelles in response to acidic conditions (pH=5.0), alkaline conditions (pH=9.0), or in the presence of esterase (60 U/mL) was measured by DLS. At different time points, the hydrolysis product was collected for ^{1}H NMR. Moreover, the final product was dialyzed using a MWCO 1000 Membrane to test ESI-MS.

DTPA/Gd release rate from APC-DTPA/Gd

Dialysis method was applied to characterize DTPA/Gd release from the APC-DTPA/Gd micelle under acidic conditions (pH=5.0), alkaline conditions (pH=9.0), or in the presence of esterase (60 U/mL). 3 mL buffer and 1 mL of APC-DTPA/Gd micelle solution were put into a dialysis bag (MWCO: 3500) in a 37 °C water bath. The Gd^{3+} concentration was measured by ICP-OES via sampling 0.5 mL solution outside of the dialysis bag at specified times.

Cytotoxicity assessment *in vitro*

The cytotoxicity of APC and APC-DTPA/Gd were assessed in Hela and 4T1 cells using MTT assays. In a typical process, cells plated in 96-well plates were allowed to grow to >70% confluence. After rinsing with PBS buffer, cells were cultured in serum-free medium with different concentrations of APC and APC-DTPA/Gd for 24 h. Then, serum-free medium (100 μL) containing thiazolyltetrazolium (0.5 mg/mL) was added after twice washing with PBS buffer, and the cells were cultured for another 4 h. After medium was removed, dimethyl sulfoxide (200 μL) was used to dissolve the purple crystal converted from thiazolyltetrazolium by living cells. Finally, the absorption at 570 nm was measured by a microplate reader (M200-PRO Tecon).

Long-term toxicity evaluation of APC and APC-DTPA/Gd

Balb/c mice (~20 g) were intravenously injected with APC and APC-DTPA/Gd (150 μL, 2 mg/mL). Mice as a control group were fed with the same condition but injected with saline. Their body weight and daily behaviour, including eating, drinking, sleeping, urination, climbing and exploratory behaviour were monitored every 1 week.

For biochemistry and histopathology assessment, the mice were sacrificed 30 days after administration with APC and APC-DTPA/Gd. The blood was subjected to blood biochemistry analysis. The major organs were fixed and used for histological evaluation (H&E staining).

Biodistribution analysis of APC-DTPA/Gd

For biodistribution, 150 μL solution of APC-DTPA/Gd was injected intravenously into the mice. After different times, the major organs were collected for measuring the Gd amount by ICP-OES. In brief, the organs were lyophilized, weighed and digested in sequence. By comparing the Gd element content, the percentage of added dose per gram (%ID/g) for each organ was obtained.

Building the xenograft tumor model

The 4T1 (breast cancer) xenograft tumor model: Balb/c mice (~20 g) were subcutaneously injected with a cell suspension having 1×10^6 4T1 cells.

The A2780 (ovarian cancer) xenograft tumor model: Balb/c nude mice (~20 g) were subcutaneously injected with a cell suspension having 1×10^6 A2780 cells.

T_1-weighted MRI *in vitro* and *in vivo*

A series of various concentrations of APC-DTPA/Gd was measured using a 9.4 T Bruker avance III 400 MHz NMR spectrometer to get T_1 relaxation times. Phantom MR Images were obtained using a 3.0 T MRI apparatus (SIEMENS MAGNETOM Avanto). For *in vivo* T_1-weighted MRI, the mice were firstly anesthetized by intraperitoneal injection using 10 % w/w of chloral hydrate solution, and then 150 μL of APC-DTPA/Gd aqueous solution was injected via the tail vein. The mice were scanned pre- and post-injection at different time points. Parameters: TE = 10 ms, TR = 369 ms, FOV read = 230 mm × 230 mm, slice thickness = 2 mm. The MR signal was measured using Image J software.

Results and Discussion

Systhesis and charaterisation of APC-DTPA/Gd

The APC-DTPA/Gd micelles were synthesized as detailed in the supplementary materials (Figure S1) [30]. Firstly, the triblock copolymer poly (allylglycidylether carbonate)-b-poly(propylene carbonate)-poly(allylglycidylether carbonate) (PAGEC-b-PPC-b-PAGEC) was prepared by sequential epoxide addition copolymerization reaction. Notably, to accurately calculate the molecular weight (M_n) of the resulting polymers, sebacic acid was chosen as starter under the catalysis of binary salen Co TFA/PPNTFA catalyst [32, 33]. The resulting absolute M_n was comparable to

that measured by GPC with a narrow polydispersity index (PDI) (Table S1), reflecting precise control. The average degree of polymerization of triblock copolymer was selected as 40/40 for PAGEC/PPC according to the integration area of the ^{1}H NMR spectra (Figure S2-4). Then, triblock copolymer was connected with cysteine via thiol-ene click chemistry. From the ^{1}H NMR spectra in Figure S5-6, all of the allyl groups were converted into Boc-protected amino acid groups. Then, Boc deprotection was conducted, giving the corresponding tri-block amphiphilic polycarbonates (APC) (Figure S7). Despite the fact that salen Co complex is a colored toxic catalyst, the inductively coupled plasma-optical emission spectrometer (ICP-OES) result and the white polymer proved non-metal residual (Figure S7). Subsequently, the resulting APCs were labeled with gadolinium to afford APC-DTPA/Gd after reacting with diethylene-etriaminopentaacetic acid (DTPA) dianhydride as the chelating agent (Figure S8).

After purification, the block copolymers carring DTPA/Gd can self-assemble into polymeric micelles (Figure 1A). To ensure the stability of the assembled micelles, the critical micelle concentrations (CMC) of APC and APC-DTPA/Gd were measured by pyrene fluorescent probe approach and fitted using Boltzamann analytical method. As demonstrated in Figure S9, the CMC of APC and APC-DTPA/Gd were 32.56 mg/L and 53.86 mg/L, respectively. The mechanism of self-assembly was attributed to the driving force that reduced the interfacial energy by the balance between the hydrophilic block and the hydrophobic block [34-36]. According to transmission electron microscopy (TEM) and dynamic light scattering (DLS) results, APC and APC-DTPA/Gd showed quite narrowly distributed spherical morphology (Figure 1B, S10-12). The mean size of APC NPs was 38 nm, while that of APC-DTPA/Gd was enhanced to 71 nm due to the surface modification of DTPA/Gd. Because of the shrinkage of the nanoparticles prepared for TEM and high hydrophilic ability of DTPA/Gd, the hydrodynamic diameter of APC-DTPA/Gd was ~200-300 nm in water, which can extravasate into tumor interstitium via leaky vasculature [37, 38]. The elemental mapping of APC-DTPA/Gd confirmed the presence of Gd elements in the self-assembled polymeric micelles (Figure 1C). ^{1}H NMR and FTIR were also carried out to verify the structure of the product (Figure S8, S13, respectively). As revealed by the ^{1}H NMR spectrum of APC-DTPA, the peaks at 2.6-3.8 ppm belonged to the protons of DTPA [39, 40]. According to the integration of protons

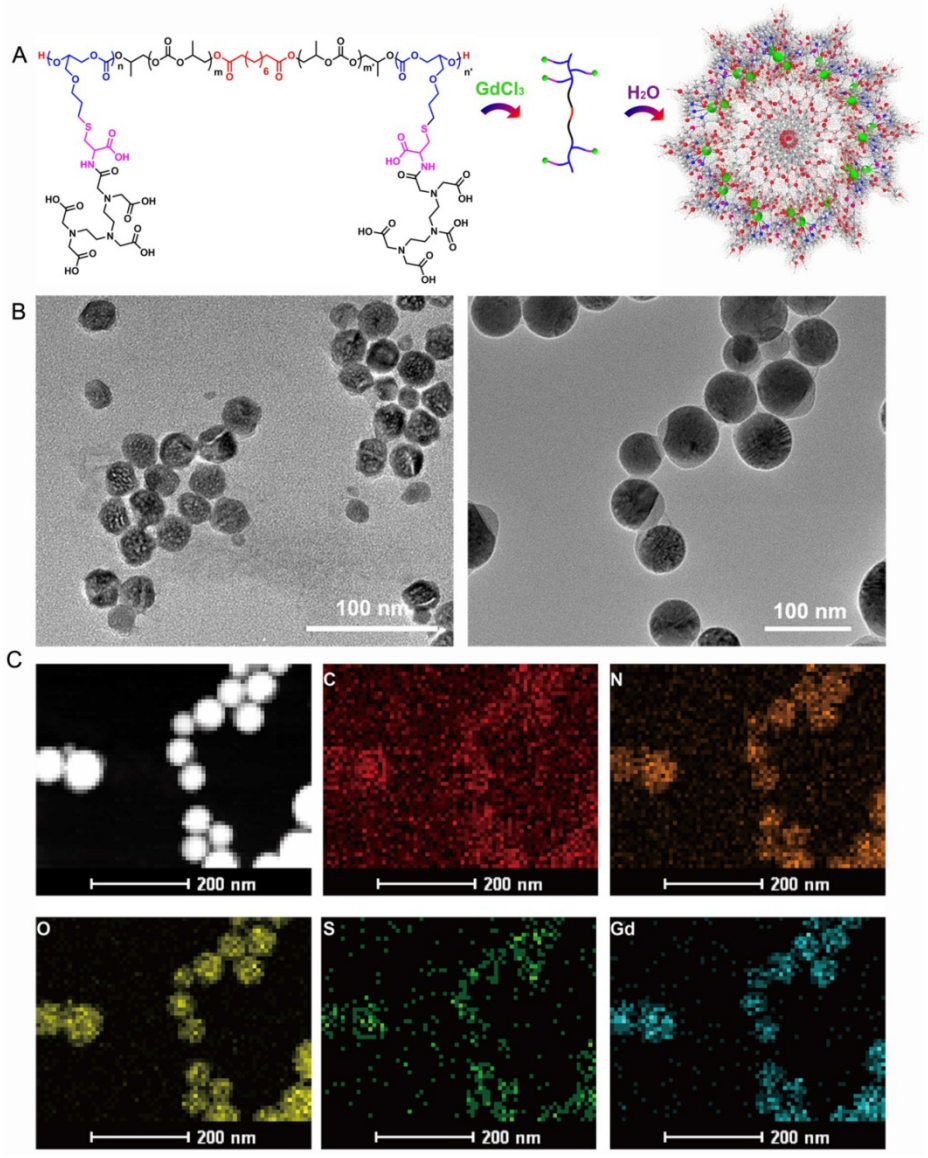

Figure 1. (A) Schematic illustration of the synthesis of APC-DTPA/Gd. (B) TEM of (left) APC and (right) APC-DTPA/Gd. (C) Energy-dispersive spectroscopy (EDS) mapping images of APC-DTPA/Gd.

from DTPA and APC, about 45.6% of DTPA was grafted onto the APC side chain. After adding Gd^{3+}, the band at 1625 cm^{-1} ascribed to the C=O stretching vibration shifted to a lower wavelength, implying the coordination of Gd^{3+} [41]. The amount of Gd within the sample was determined to be 37.14 wt% (42.8 mol%) by ICP-OES. To assess the paramagnetic properties of the Gd-conjugated APC, T_1-weighted MR images (Figure 2A) were recorded, which brightened with increasing concentration of Gd. The relaxivity (r_1) was then calculated to be 11.1 $mM^{-1}·s^{-1}$, 2.4× higher than that of commercial DTPA-Gd (3.3 $mM^{-1}·s^{-1}$) at a 9.4 T (400MHz) magnetic field strength (Figure 2B). Based on the Solomon-Bloembergen-Morgan theory, the rather higher r_1 of APC-DTPA/Gd may be caused by decreased themolecular tumbling rates and increased ionic relaxivity rate in the confined space of nanomaterials [42]. The two key factors, mean residence lifetime and rotational correlation time, play a great role in determining optimal relaxivity. This result (r_1 = 11.1 $mM^{-1}·s^{-1}$) was lower than the restricted systems where the Gd was placed at the barycenter of the carrier [43, 44] or self-assembled by metal templated approach [45]. However, the increased relaxivity was comparable to other Gd-polymer systems with different carrier topologies such as linear [46, 47], dentrimer [48, 49], star [50] and hyperbranched [51]. Therefore, this amphiphilic APC-DTPA/Gd system was advantageous for the enhancement of r_1 relaxivity and application in MR imaging.

The biocompatibility of APC and APC-DTPA/Gd *in vitro* and *in vivo*

To explore the potential application of CO_2-based APC in biomedicine, we first investigated the biocompatibility and biodegradability of APC and APC-DTPA/Gd. APC and APC-DTPA/Gd micelles showed relatively low cytotoxicity to the Hela and 4T1 cells even at high concentration after 24 h treatment (Figure 3A). This is especially beneficial for the micelles to function as a probe that does not induce nonspecific cytotoxicity. Furthermore, the *in vivo* toxicity of the APC and APC-DTPA/Gd was tested by histopathologic diagnosis and blood chemical analyses (Figure 3B-E, Table S2). Body weight did not show a noticeable drop in the APC-treated and APC-DTPA/Gd -treated groups over a 1 month period. Organs of the experimental mice did not show remarkable lesions or abnormalities compared with those of the control group. Hematoxylin and Eeosin (H&E) staining revealed no significant interference with immune response or the physiological regulation of haem. Concentrations of five important hepatic indicators – albumin (ALB), aspartate transaminase (AST), total protein (TP), alanine transaminase (ALT), and alkaline phosphatase (ALP) – fell in a normal range and suggested negligible liver injury. Our results collectively evidenced that APC and APC-DTPA/Gd were not appreciably toxic to mice at our injected dose (15 mg/kg) after systemic administration. Considering the biocompatible and amphiphilic features of APC, we preliminarily investigated its drug loading ability. 7-ethyl-10-hydroxyl-camptothecin (SN38) was selected as the hydrophobic model drug, which is a potent topoisomerase I inhibitor for cancer chemotherapy [52, 53]. After SN-38 loading, the APC-SN38 micelles formed particles ~200-300 nm in diameter (Figure 2C, 2D). As expected, APC-SN38 showed a higher anticancer ability than free SN-38 at the same concentration, which suggested that the APC can realize drug loading and improve anticancer ability (Figure 2E).

Biodegradability of APC and APC-DTPA/Gd *in vitro*

The acidic environment of endo/lysosomes and high esterase activity in the liver enable the decomposition of ester bonds *in vivo* [54]. To simulate the biodegradability of APC-DTPA/Gd micelles, hydrolysis experiments under acidic conditions (pH = 5.0), alkaline conditions (pH = 9.0), or in the presence of esterase (60 U/mL) were performed *in vitro*. Upon incubation in the above conditions, the size of the micelles increased and their size distribution became broader, suggesting that the micelles were destabilized due to degradation of their backbone (Figure S14-16). ^1H NMR and electrospray ionisation mass spectrometry (ESI-MS) spectra confirmed the production of cyclic carbonate species that were non-acidic and non-toxic to the body during hydrolysis of APC (Figure 4C, S17-20) [55]. According to the integral area of H from cycle carbonic ester and cysteine (Figure S18-S20), the production ratio of cycle carbonic ester is demonstrated in Figure 4D. Furthermore, small molecular Gd was released from APC-DTPA/Gd micelles in the form of DTPA-Gd complex (Figure 4, S21), which could decrease the risk of nephrogenic systemic fibrosis (NSF) caused by free Gd and partly increase the biocompatibility of the degraded polymer. In addition, *in vivo* investigations were carried out to quantitatively analyze the Gd content in the major organs by ICP-OES. Experimental results showed that the intravenously administered APC-DTPA/Gd micelles largely accumulated in the liver, spleen and kidneys, but they were noticeably cleared from the body in 72 h (Figure 5A-B). The evidence that Gd could be detected in the urine

strongly suggests the renal clearance of APC-DTPA/Gd micelles (Figure 5D). Importantly, the relative quick excretion of APC-DTPA/Gd *in vivo* decreases the chances of trans-metalation between Gd^{3+} and endogenous metal ions, such as Zn^{2+}, Cu^{2+}, and Ca^{2+}, avoiding the release of free Gd^{3+} [56]. Moreover, there was scarcely any Gd^{3+} residue in the body after 5 day and 10 days, measured by ICP-OES and ICP-MS (Table S3). Together, these results confirmed that APC-DTPA/Gd micelles could be degraded into harmless products and could be effectively cleared from the body in a relatively short time, ensuring they can act as carriers for tumor imaging.

The MRI ability of APC-DTPA/Gd for tumor imaging and their *in vivo* metabolism

These inspiring outcomes stimulated us to assess the feasibility of APC-DTPA/Gd micelles as MRI probes *in vivo*. A solution of APC-DTPA/Gd micelles was intravenously administered to balb/c mice bearing 4T1 tumors and whole-body MR images were recorded at timed intervals (Figure 6A, S22). The T_1 signals from the tumor sites revealed a change in the contrast enhancement over 72 h, with the optimal contrast of the MRI signal observed at 24 h. In contrast to APC-DTPA/Gd micelles, intravenous injection of commercial DTPA/Gd complex failed to improve T_1 contrast enhancement in the tumor region. We further validated the suitability of the APC-DTPA/Gd toward tumor with different volumes and types (Figure 6 B-E). Balb/c mice bearing small 4T1 xenograft tumors and balb/c nude mice bearing A2780 xenograft tumors were administrated with DTPA/Gd and APC-DTPA/Gd. The MR signal from the tumor in mice injected with APC-DTPA/Gd was higher than that in mice injected with DTPA/Gd. These results strongly suggested that the superior MR imaging capability of APC-DTPA/Gd micelles could be utilized to monitor in real-time their targeting and accumulation toward tumors through enhanced permeability and retention (EPR) effects *in vivo* [57-59]. Moreover, the terminal disposition half-life ($t_{1/2}$) values of APC-DTPA/Gd and DTPA/Gd were 6.4 h and 0.22 h respectively, revealing that APC-DTPA/Gd micelles were capable of extending the circulation of Gd in the bloodstream, while commercial DTPA/Gd was rapidly cleared from plasma (Figure 5C).

In vivo biodistribution and clearance of intravenously injected APC-DTPA/Gd micelles was demonstrated using MR imaging (Figure 7). As with many other nanomaterials, an initial signal increase was mainly observed in the MPS-associated organs such as the liver [60, 61]. A more careful look at coronal scanning revealed that both kidney and bladder also showed strong signal, suggesting that APC-DTPA/Gd micelles were primarily excreted through renal filtration. As discussed above, the mechanism of clearance is attributed to degradation of APC-DTPA/Gd micelles into small molecule products followed by renal excretion. At 72 h post-injection, the signal in the liver, kidney and bladder recovered to the pre-injection levels, indicating that the injected APC-DTPA/Gd was completely cleared from the body. These *in vivo* results demonstrated that APC-DTPA/Gd micelles not only manifested effective tumor diagnosis ability, but also their renal clearance characteristic decreased their persistence in the body and eliminated the hazards of long-term toxicity.

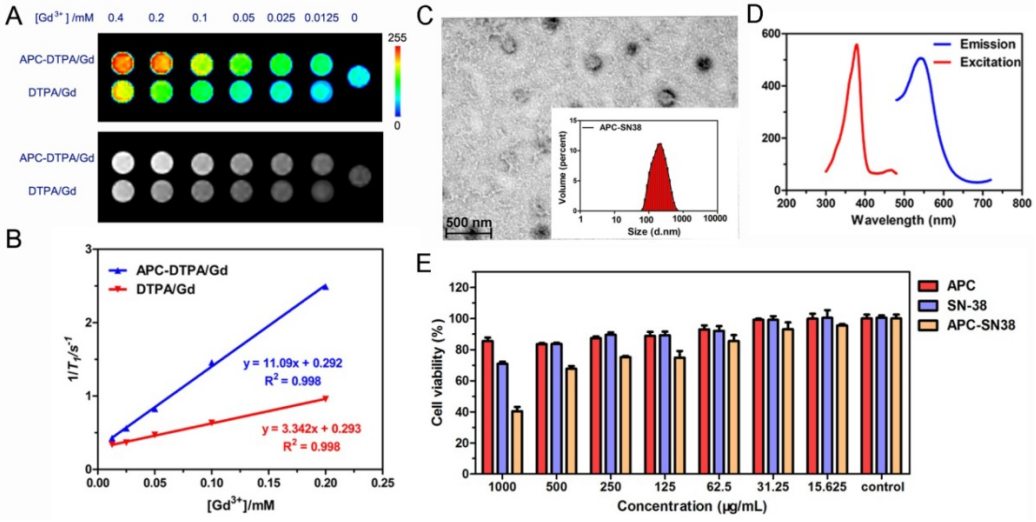

Figure 2. (A) T_1-weighted MR images and (B) the relaxation rate of APC-DTPA/Gd vs. different concentrations of Gd^{3+}. (C) TEM and (D) fluorescence spectra of APC-SN38. (E) The cell viability of HeLa cells in the presence of APC, free SN-38 and APC-SN38 under varied concentrations.

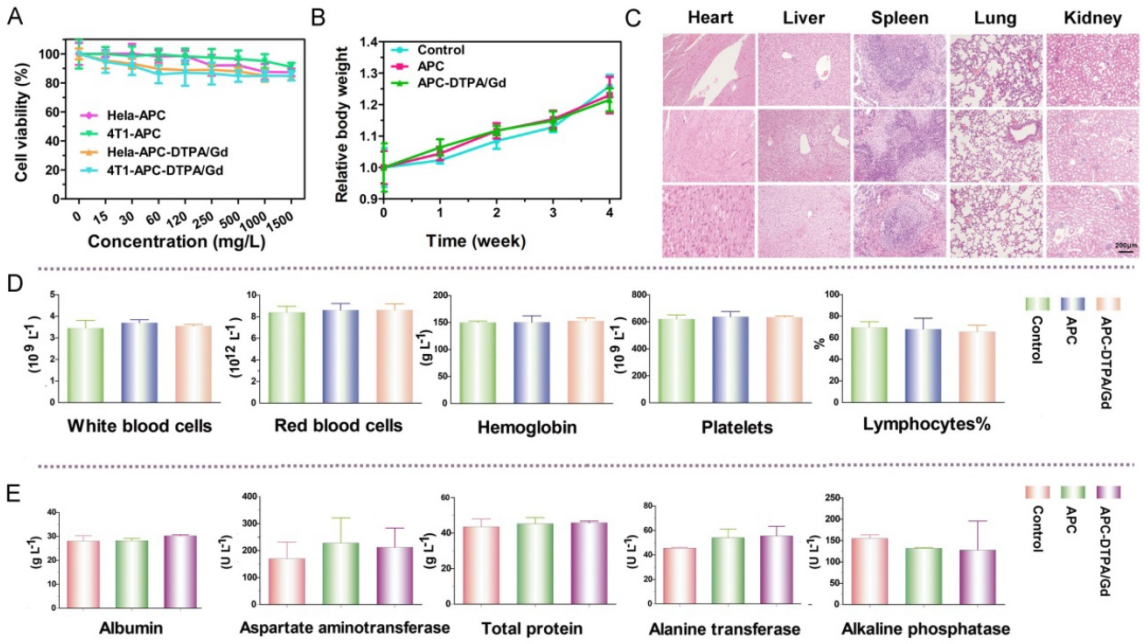

Figure 3. (A) Cell viability of cells after incubation with increasing concentrations of APC and APC-DTPA/Gd. (B) Relative body weight of mice with different treatments. (C) H&E stained slices of major organs from mice treated with (top) saline, (middle) APC, and (bottom) APC-DTPA/Gd (The scale bar indicates 200 μm). (D) Blood analysis data and (E) liver-function test of different treatments (n=3).

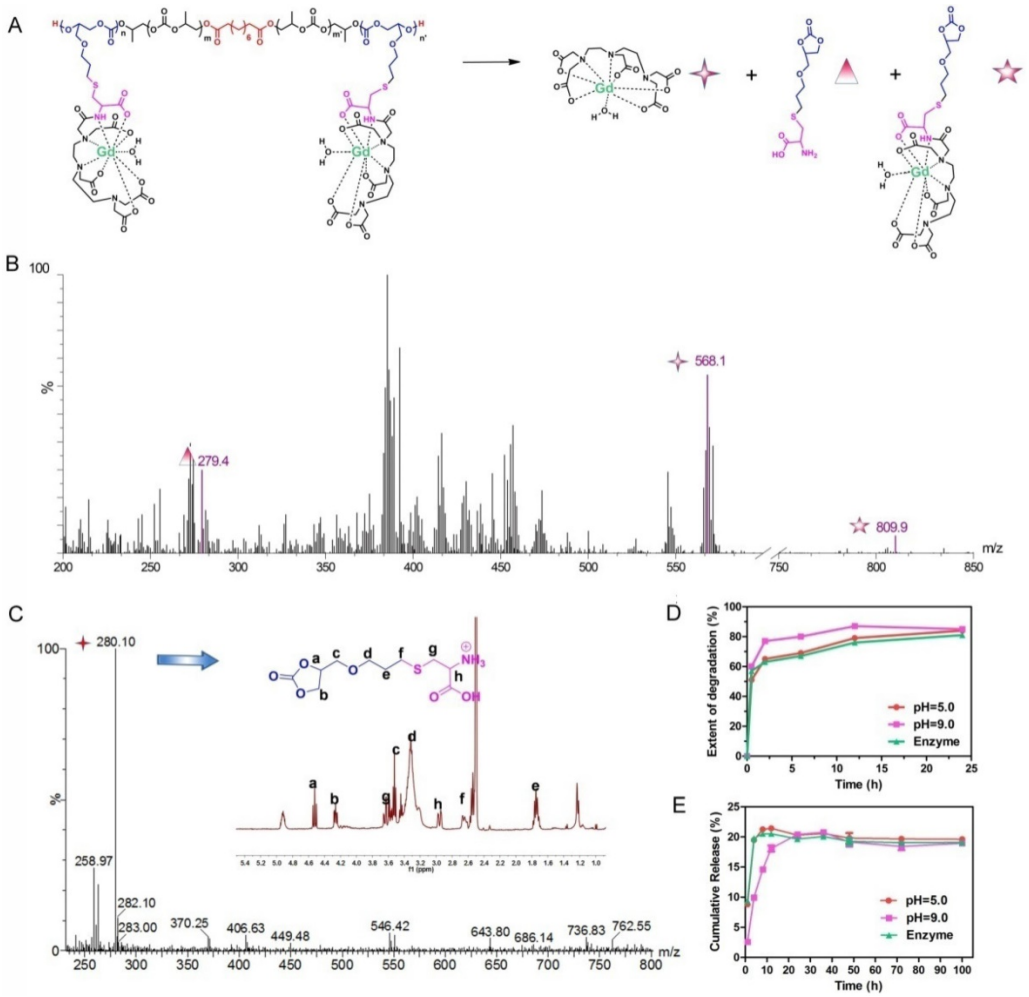

Figure 4. (A) The depolymerization process and ESI-MS spectra of APC-DTPA/Gd. (C) The ^{1}H NMR and ESI-MS spectra of cyclic carbonate produced by APC depolymerization. (D) The depolymerization of APC and (E) Gd release from APC-DTPA/Gd under different conditions.

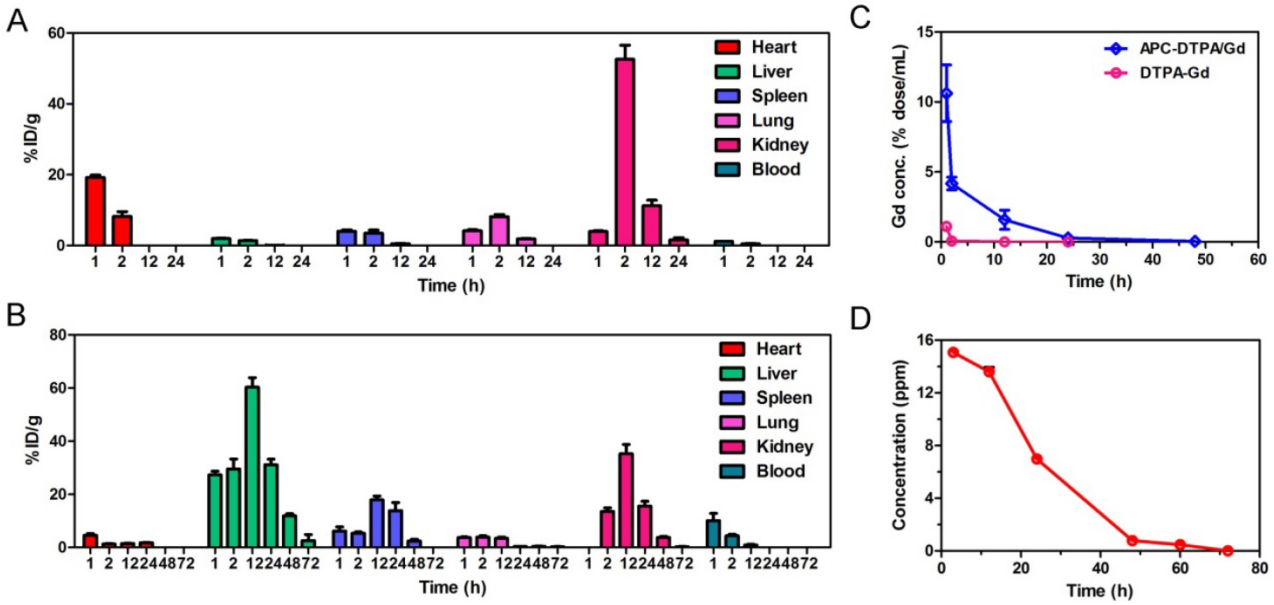

Figure 5. Time dependent biodistribution of Gd^{3+} in organs of DTPA/Gd (A) and APC-DTPA/Gd (B). (C) The biodistribution of Gd^{3+} in the blood. (D) The concentration of Gd^{3+} in the urine after injection of APC-DTPA/Gd.

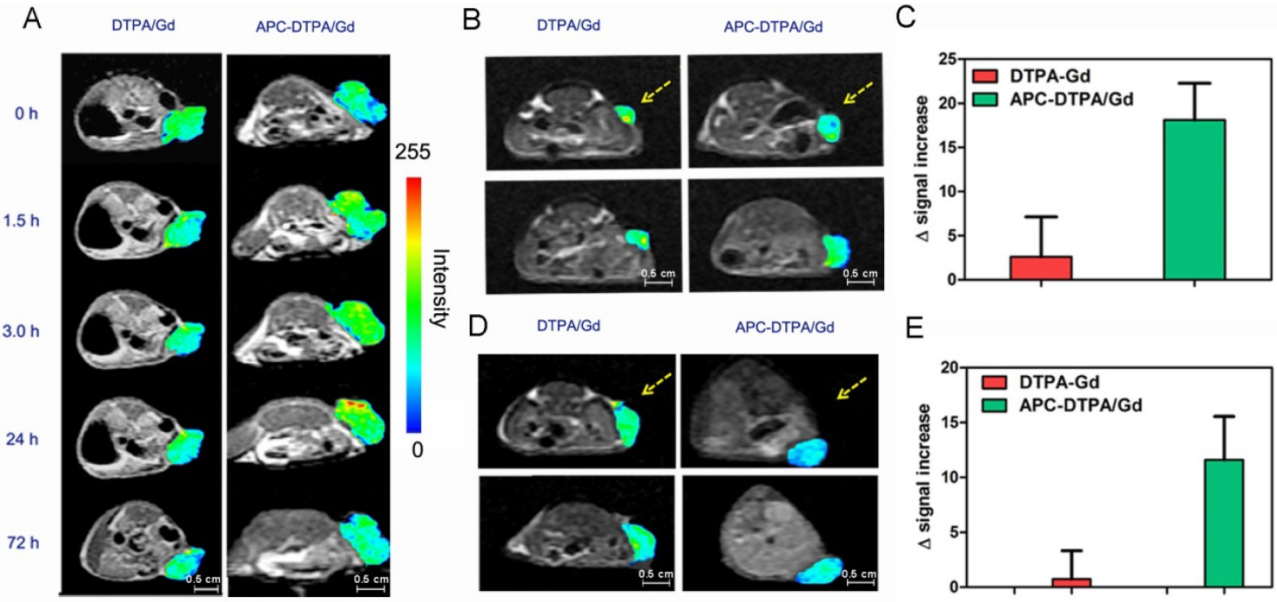

Figure 6. *In vivo* T_1-weighted MR images of a (A) large 4T1 tumor-bearing mouse before and after intravenous injection of DTPA-Gd and APC-DTPA/Gd. *In vivo* T_1-weighted MR images and signal enhancement of mice bearing (B, C) small 4T1 and (D, E) A2780 tumors before and after intravenous injection of DTPA-Gd and APC-DTPA/Gd. The pseudo colors indicate the tumor sites.

Conclusions

In this study, we have provided a new kind of biodegradable CO_2-based APC for tumor imaging *in vivo*. Through conjugation of APC with Gd, the resulting APC-DTPA/Gd polymeric micelles exhibit good MRI performance. Furthermore, the APC-DTPA/Gd are mainly found in MPS-related organs and can be degraded into renally cleared products within a reasonable timescale without evidence of toxicity. This emerging class of low-toxicity biodegradable CO_2-based APC can provide a powerful platform for clinical transition.

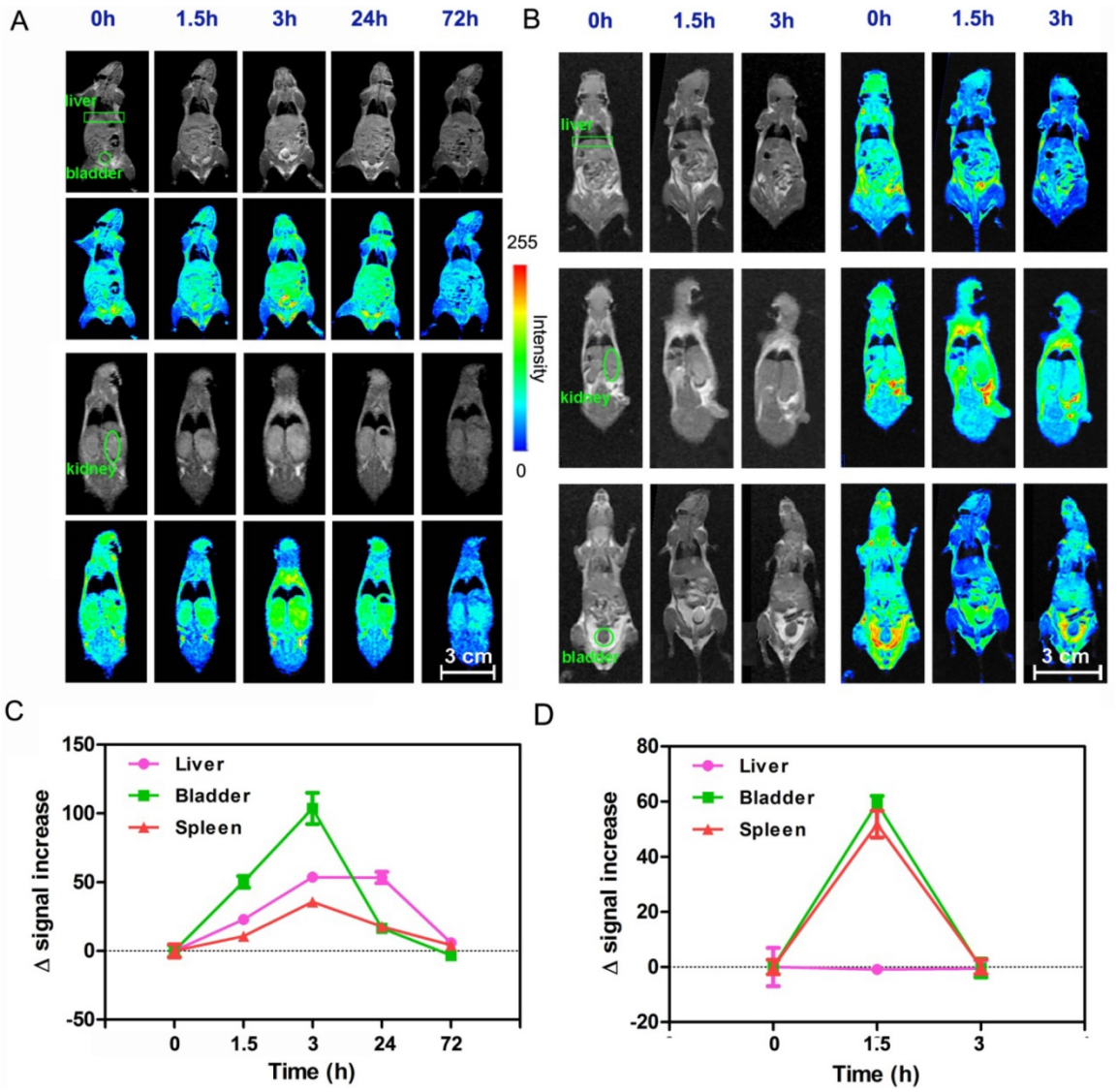

Figure 7. *In vivo* MR imaging of the liver (rectangles), bladder (circle) and kidney (ellipses) after intravenous injection of (A) APC-DTPA/Gd and (B) DTPA/Gd at different time points. *In vivo* MR signal varied after injection of (C) APC-DTPA/Gd and (D) DTPA/Gd at different time points.

Abbreviations

FDA: Food and Drug Administration; APC: amphiphilic polycarbonates; Gd: gadolinium; MPS: mononuclear phagocytic system; MR: magnetic resonance; CMC: critical micelle concentration; TEM: transmission electron microscopy; DLS: dynamic light scattering; SN38: 7-ethyl-10-hydroxyl-camptothecin; EPR: enhanced permeability and retention.

Acknowledgments

This work was supported by the National Natural Science Foundation of China (grant no. 21635007, 51321062, 21721003).

Supplementary Material

Supplementary figures and tables.
http://www.thno.org/v07p4689s1.pdf

Competing Interests

The authors have declared that no competing interest exists.

References

1. Elsabahy M, Heo GS, Lim SM, et al. Polymeric nanostructures for imaging and therapy. Chem Rev. 2015; 115: 10967-1011.
2. Liu Y, Ai K, Ji X, et al. Comprehensive insights into the multi-antioxidative mechanisms of melanin nanoparticles and their application to protect brain from injury in ischemic stroke. J Am Chem Soc. 2017; 139: 856-62.
3. Khlebtsov N, Dykman L. Biodistribution and toxicity of engineered gold nanoparticles: a review of in vitro and in vivo studies. Chem Soc Rev. 2011; 40: 1647-71.
4. Liu Y, Ai K, Liu J, et al. Dopamine-melanin colloidal nanospheres: an efficient near-infrared photothermal therapeutic agent for in vivo cancer therapy. Adv Mater. 2013; 25: 1353-9.
5. Lewinski N, Colvin V, Drezek R. Cytotoxicity of nanoparticles. Small. 2008; 4: 26-49.
6. Longmire M, Choyke PL, Kobayashi H. Clearance properties of nano-sized particles and molecules as imaging agents: considerations and caveats. Nanomedicine (Lond). 2008; 3: 703-17.
7. Choi HS, Liu W, Misra P, et al. Renal clearance of quantum dots. Nat Biotechnol. 2007; 25: 1165-70.

8. Choi HS, Liu W, Liu F, et al. Design considerations for tumour-targeted nanoparticles. Nat Nanotechnol. 2010; 5: 42-7.
9. Zhou M, Li J, Liang S, et al. CuS nanodots with ultrahigh efficient renal clearance for positron emission tomography imaging and image-guided photothermal therapy. ACS Nano. 2015; 9: 7085-96.
10. Xing H, Zhang S, Bu W, et al. Ultrasmall $NaGdF_4$ nanodots for efficient MR angiography and atherosclerotic plaque imaging. Adv Mater. 2014; 26: 3867-72.
11. Yu M, Liu J, Ning X, et al. High-contrast noninvasive imaging of kidney clearance kinetics enabled by renal clearable nanofluorophores. Angew Chem Int Ed. 2015; 54: 15434-8.
12. Park JH, Gu L, Von Maltzahn G, et al. Biodegradable luminescent porous silicon nanoparticles for in vivo applications. Nat Mater. 2009; 8: 331-6.
13. Chou LY, Zagorovsky K, Chan WC. DNA assembly of nanoparticle superstructures for controlled biological delivery and elimination. Nat Nanotechnol. 2014; 9: 148-55.
14. Sun L, Li X, Wei X, et al. Stimuli-responsive biodegradable hyperbranched polymer-gadolinium conjugates as efficient and biocompatible nanoscale magnetic resonance imaging contrast agents. ACS Appl Mater Interfaces. 2016; 8: 10499-512.
15. Jin H, Huang W, Zhu X, et al. Biocompatible or biodegradable hyperbranched polymers: from self-assembly to cytomimetic applications. Chem Soc Rev. 2012; 41: 5986-97.
16. Ye M, Qian Y, Tang J, et al. Targeted biodegradable dendritic mri contrast agent for enhanced tumor imaging. J Control Release. 2013; 169: 239-45.
17. Nair LS, Laurencin CT. Biodegradable polymers as biomaterials. Prog Polym Sci. 2007; 32: 762-98.
18. Tian H, Tang Z, Zhuang X, et al. Biodegradable synthetic polymers: preparation functionalization and biomedical application. Prog Polym Sci. 2012; 37: 237-80.
19. Liu SQ, Yang C, Huang Y, et al. Antimicrobial and antifouling hydrogels formed in situ from polycarbonate and poly(ethylene glycol) via michael addition. Adv Mater. 2012; 24: 6484-9.
20. Fukushima K. Poly(trimethylene carbonate)-based polymers engineered for biodegradable functional biomaterials. Biomater Sci. 2016; 4: 9-24.
21. Tempelaar S, Mespouille L, Coulembier O, et al. Synthesis and post-polymerisation modifications of aliphatic poly(carbonate)s prepared by ring-opening polymerisation. Chem Soc Rev. 2013; 42: 1312-36.
22. Chan JM, Ke X, Sardon H, et al. Chemically modifiable N-heterocycle-functionalized polycarbonates as a platform for diverse smart biomimetic nanomaterials. Chem Sci. 2014; 5: 3294-300.
23. Ulery BD, Nair LS, Laurencin CT. Biomedical applications of biodegradable polymers. J Polym Sci Part B Polym Phys. 2011; 49: 832-64.
24. Thomas AW, Dove AP. Postpolymerization modifications of alkene-functional polycarbonates for the development of advanced materials biomaterials. Macromol Biosci. 2016; 16: 1762-75.
25. Feng J, Zhuo RX, Zhang XZ. Construction of functional aliphatic polycarbonates for biomedical applications. Prog Polym Sci. 2012; 37: 211-36.
26. Chen W, Meng F, Cheng R, et al. Advanced drug and gene delivery systems based on functional biodegradable polycarbonates and copolymers. J Control Release. 2014; 190: 398-414.
27. Darensbourg DJ, Wei SH, Yeung AD, et al. An efficient method of depolymerization of poly(cyclopentene carbonate) to its comonomers: cyclopentene oxide and carbon dioxide. Macromolecules. 2013; 46: 5850-5.
28. Darensbourg DJ, Wei SH. Depolymerization of polycarbonates derived from carbon dioxide and epoxides to provide cyclic carbonates, a kinetic study. Macromolecules. 2012; 45: 5916-22.
29. Lu XB, Darensbourg DJ. Cobalt catalysts for the coupling of CO_2 and epoxides to provide polycarbonates and cyclic carbonates. Chem Soc Rev. 2012; 41: 1462-84.
30. Wang Y, Fan J, Darensbourg DJ. Construction of versatile and functional nanostructures derived from CO_2-based polycarbonates. Angew Chem Int Ed. 2015; 54: 10206-10.
31. Han SS, Li ZY, Zhu JY, et al. Dual-pH sensitive charge-reversal polypeptide micelles for tumor-triggered targeting uptake and nuclear drug delivery. Small. 2015; 11: 2543-54.
32. Gao Y, Gu L, Qin Y, et al. Dicarboxylic acid promoted immortal copolymerization for controllable synthesis of low-molecular weight oligo(carbonate-ether) diols with tunable carbonate unit content. J Polym Sci Part A Polym Chem. 2012; 50: 5177-84.
33. Liu S, Miao Y, Qiao L, et al. Controllable synthesis of a narrow polydispersity CO_2-based oligo(carbonate-ether) tetraol. Polym Chem. 2015; 6: 7580-5.
34. Duan Z, Zhang Y, Zhu H, et al. Stimuli-sensitive biodegradable and amphiphilic block copolymer-gemcitabine conjugates self-assemble into a nanoscale vehicle for cancer therapy. ACS Appl Mater Interfaces. 2017; 9: 3474-86.
35. Li N, Cai H, Jiang L, et al. Enzyme-sensitive and amphiphilic PEGylated dendrimer-paclitaxel prodrug-based nanoparticles for enhanced stability and anticancer efficacy. ACS Appl Mater Interfaces. 2017; 9: 6865-77.
36. Yang Y, Pan D, Luo K, et al. Biodegradable and amphiphilic block copolymer-doxorubicin conjugate as polymeric nanoscale drug delivery vehicle for breast cancer therapy. Biomaterials. 2013; 34: 8430-43.
37. Peer D, Karp JM, Hong S, et al. Nanocarriers as an emerging platform for cancer therapy. Nat Nanotechnol. 2007; 2: 751-60.
38. Wang S, Huang P, Chen X. Hierarchical targeting strategy for enhanced tumor tissue accumulation/retention and cellular internalization. Adv Mater. 2016; 28: 7340-64.
39. Turner JL, Pan D, Plummer R, et al. Synthesis of gadolinium-labeled shell-crosslinked nanoparticles for magnetic resonance imaging applications. Adv Funct Mater. 2005; 15: 1248-54.
40. Zhang L, Liu T, Xiao Y, et al. Hyaluronic acid-chitosan nanoparticles to deliver Gd-DTPA for MR cancer imaging. Nanomaterials (Basel). 2015; 5: 1379-96.
41. Li L, Tong R, Li M, et al. Self-assembled gemcitabine-gadolinium nanoparticles for magnetic resonance imaging and cancer therapy. Acta Biomater. 2016; 33: 34-9.
42. Caravan P. Strategies for increasing the sensitivity of gadolinium based MRI contrast agents. Chem Soc Rev. 2006; 35: 512-23.
43. Liu Q, Chen S, Chen J, et al. An asymmetrical polymer vesicle strategy for significantly improving T1 MRI sensitivity and cancer-targeted drug delivery. Macromolecules. 2015; 48: 739-49.
44. Hu X, Liu G, Li Y, et al. Cell-penetrating hyperbranched polyprodrug amphiphiles for synergistic reductive milieu-triggered drug release and enhanced magnetic resonance signals. J Am Chem Soc. 2014; 137: 362-8.
45. Mi P, Cabral H, Kokuryo D, et al. Gd-DTPA-loaded polymer-metal complex micelles with high relaxivity for MR cancer imaging. Biomaterials. 2013; 34: 492-500.
46. Casali C, Janier M, Canet E, et al. Evaluation of Gd-DOTA-labeled dextran polymer as an intravascular MR contrast agent for myocardial perfusion. Acad Radiol. 1998; 5: S214-S8.
47. Li X, Sun L, Wei X, et al. Stimuli-responsive biodegradable and gadolinium-based poly [N-(2-hydroxypropyl) methacrylamide] copolymers: their potential as targeting and safe magnetic resonance imaging probes. J Mater Chem B. 2017; 5: 2763-74.
48. Luo K, Liu G, She W, et al. Gadolinium-labeled peptide dendrimers with controlled structures as potential magnetic resonance imaging contrast agents. Biomaterials. 2011; 32: 7951-60.
49. Cheng Z, Thorek D, Tsourkas A. Gadolinium-conjugated dendrimer nanoclusters as a tumor-targeted T1 magnetic resonance imaging contrast agent. Angew Chem Int Ed. 2010; 49: 346-50.
50. Liu T, Li X, Qian Y, et al. Multifunctional pH-disintegrable micellar nanoparticles of asymmetrically functionalized β-cyclodextrin-based star copolymer covalently conjugated with doxorubicin and DOTA-Gd moieties. Biomaterials. 2012; 33: 2521-31.
51. Guo C, Sun L, Cai H, et al. Gadolinium-labeled biodegradable dendron-hyaluronic acid hybrid and its subsequent application as a safe and efficient magnetic resonance imaging contrast agent. ACS Appl Mater Interfaces. 2017; 9: 23508-19.
52. Liu Z, Robinson JT, Sun X, et al. PEGylated nanographene oxide for delivery of water-insoluble cancer drugs. J Am Chem Soc. 2008; 130: 10876-7.
53. Wang J, Sun X, Mao W, et al. Tumor redox heterogeneity-responsive prodrug nanocapsules for cancer chemotherapy. Adv Mater. 2013; 25: 3670-6.
54. Qiu N, Liu X, Zhong Y, et al. Esterase-activated charge-reversal polymer for fibroblast-exempt cancer gene therapy. Adv Mater. 2016; 28: 10613-22.
55. Tsai FT, Wang Y, Darensbourg DJ. Environmentally benign CO_2-based copolymers: degradable polycarbonates derived from dihydroxybutyric acid and their platinum-polymer conjugates. J Am Chem Soc. 2016; 138: 4626-33.
56. Zhang G, Zhang R, Melancon MP, et al. The degradation and clearance of poly (N-hydroxypropyl-L-glutamine)-DTPA-Gd as a blood pool MRI contrast agent. Biomaterials. 2012; 33: 5376-83.
57. Maeda H, Wu J, Sawa T, et al. Tumor vascular permeability and the EPR effect in macromolecular therapeutics: a review. J Control Release. 2000; 65: 271-84.
58. Fang J, Nakamura H, Maeda H. The EPR effect: unique features of tumor blood vessels for drug delivery factors involved and limitations and augmentation of the effect. Adv Drug Deliver Rev. 2011; 63: 136-51.
59. Shi J, Kantoff PW, Wooster R, et al. Cancer nanomedicine: progress challenges and opportunities. Nat Rev Cancer. 2017; 17: 20-37.
60. Park JH, Von Maltzahn G, Zhang L, et al. Systematic surface engineering of magnetic nanoworms for in vivo tumor targeting. Small. 2009; 5: 694-700.
61. Park JH, Von Maltzahn G, Ong LL, et al. Cooperative nanoparticles for tumor detection and photothermally triggered drug delivery. Adv Mater. 2010; 22: 880-5.